Chapter 5

Exciton-Plasmon Interactions in Quantum Well Structures Near Silver Nanoparticles

Hiroaki Matsui

Additional information is available at the end of the chapter

http://dx.doi.org/10.5772/intechopen.71466

Abstract

The chapter reports photoluminescence (PL) and an energy transfer dynamic in a hybrid heterostructure consisting of an Ag nanoparticle (NP) layer and $Cd_{0.08}Zn_{0.92}O$/ZnO quantum well (QW). The observed PL quenching was closely related to electronic states of excitons confined in the QW. The PL quenching of the QW emission was only observed at low temperatures which excited carriers were radiatively recombined due to excitonic localization derived from fluctuated energy potentials in the QW. In contrast, delocalization of excitons from the QW with increasing temperature resulted in disappearance of the PL quenching. Time-resolved PL measurements revealed a decay rate of PL from the QW emission through the presence of energy transfer from the QW to Ag NP layer. The temperature-dependent energy-transfer rate was similar to that of the radiative recombination rate. The Ag NP layer surface showed a visible light absorption caused by localized surface plasmons (LSPs), which was very close to the PL peak energy of the QW. These results indicated that the excitonic recombination energy in the QW was nonradiatively transferred to Ag NP layer owing to energy resonance between the LSP and the QW. These phenomena could be explained by a surface energy transfer mechanism.

Keywords: silver, plasmon, energy transfer, exciton, quantum well

1. Introduction

Semiconductor-based quantum wells (QWs) with metallic nanostructures, such as nanodots, nanoparticles and nanogratings, have received much attention as promising hybrid structures towards fabrications of plasmon-coupled emitting devices. In particular, the energy interactions between surface plasmons (SPs) and QW emitters have been investigated in relation to exciton-plasmon coupling [1–5]. SPs can effectively capture dipole oscillator energy in QWs. As a result, spontaneous decay rates of light emissions from QWs are remarkably modified in

close proximity to metallic nanostructures [6]. These phenomena usually lead to enhancing or quenching processes. Enhanced luminescence is promoted by localized electromagnetic fields (near-fields) induced by SPs on metallic nanostructured surfaces. On the other hand, quenching of luminescence is attributed to various energy dissipation mechanisms based on plasmon damping in metals, such as plasmonic absorptions, excitonic diffusions, and electron-hole pair excitations [7–9]. Dissipation processes related to these mechanisms are more significant than the nonradiative recombination in QWs, which results in remarkable decrease of quantum efficiency of QWs. An elucidation of luminescent quenching is a key issue for the fabrications of the plasmon-based emitting devices on QWs.

Detailed investigations concerning photoluminescent (PL) quenching have been demonstrated hybrid structures of metallic nanoparticles and semiconductor quantum dots (QDs) [10–14]. The quenching effect has been utilized to bio-photonic applications such as chips for the detections of DNA, protein molecules, and energy transfer assays [15]. In the cases of Au nanoparticles (NPs)–CdSe QDs, the efficient PL quenching has been closely related to the spectral overlap of plasmon absorptions of Au NPs and light emissions from the QDs, as well as the separation length between Au nanoparticles and the QDs. The recombination energy of confined excitons in the QDs has been nonradiatively transferred to the Au NPs, leading to shortening lifetimes of light emissions from the QDs, which could be explained by both mechanisms of Förster energy transfer (FRET) [16] and surface energy transfer (SET) processes [17]. A FRET process induced between Au NPs and QDs is based on a dipole-dipole interaction between Au NPs and QDs. A dipole-dipole interaction is known as short-range coupling with d^{-6} order, where d represents separation distance between Au NPs and QDs. On the other hand, a SET process has been known as a dipole-surface energy transfer, which has long-range coupling with d^{-4} order. Therefore, difference in mechanism between FRET and SET processes is closely related to spatial distance of a field interaction.

Recently, energy coupling between QWs and SPs has been studied on $In_xGa_{1-x}N$-based and $Cd_xZn_{1-x}O$-based QWs with Ag nanostructures. Some studies demonstrated PL enhancement [18], while others reported quenched PL [19, 20]. For $In_xGa_{1-x}N$ and $Cd_xZn_{1-x}O$ alloys, it is known that electronic states in QWs are present either in the form of bound electron–hole pairs (localized excitons) or free electrons and holes (free excitons), as realized by carrier localization or delocalization, respectively. These electronic states give an influence to the quantum efficiency of $In_xGa_{1-x}N$ and $Cd_xZn_{1-x}O$ QWs, which is further dependent on temperature [21–23]. High quantum efficiency is based on excitonic localization at defect sites such as interface disorders and atom fluctuations. In the concrete cases of $In_xGa_{1-x}N$ QWs with Ag nanostructures, it was reported that the plasmon-coupled PL properties at room temperature were suppressed at low temperatures [24]. Furthermore, it was confirmed that the PL quenching became strong with increasing quantum efficiency of $In_xG_{a1-x}N$ QWs [25]. These results resulted in the conjecture that the PL quenching is closely attributed to the electronic states of $In_xGa_{1-x}N$ QWs in the presence of Ag nanostructures. However, the influence of plasmonic fields on PL quenching has, for the most part, remained undocumented at present. Accordingly, the origin of nonradiative energy transfer contributing to PL quenching is not fully understood.

In this study, I focus on $Cd_xZn_{1-x}O$ QWs with visible PL for studies of plasmon-exciton coupling. To date, we have investigated band-edge luminescence of $Cd_xZn_{1-x}O$ QWs in order to understand optical properties of excitonic recombination in the QWs [26–28].

http://dx.doi.org/10.5772/intechopen.71466

$Cd_xZn_{1-x}O$ QWs along the polar axis produce internal fields due to piezoelectric and spontaneous polarizations between well and barrier layers. In the case, we must consider two kinds of radiative processes. One process involves excitonic localization because of spatial cadmium fluctuations. The cadmium-rich regions have functions of radiative recombination centers of localized excitons at potential minima formed in $Cd_xZn_{1-x}O$ wells. The other process is related to the quantum-confinement Stark effect (QCSE) generated by an internal field induced in wells [29]. For a well whose width is greater than the excitonic Bohr diameter of the free exciton (R_{ex} = 3.6 Å in ZnO), excitonic localization is weakened by the QCSE. As a consequence, excitonic localization is enhanced by interfacial fluctuations such as interface defects and well-width variations because the excitonic wave function confined in a well penetrates into a barrier. This behavior is well observed for narrow well widths less than R_{ex}, which leads to efficient PL due to a strong radiative recombination.

This chapter reports the temperature-dependent optical dynamics of PL quenching in a $Cd_xZn_{1-x}O$ QW placed in the vicinity of Ag NP layer. The samples in this work do not exhibit PL enhancement at any temperature, which is convenient for optical studies of quenching behaviors. In our case, pulsed optical excitations are used to evaluate the dynamics of energy transfer and other competing processes concerning carrier recombination in the QW. To an effort to understand the exciton-plasmon coupling, two kinds of relaxation steps in the QW were considered, namely, radiative or nonradiative recombination of excited carriers (electrons and holes). These physical states can be alternatively realized by changing the temperature. In addition, a ZnO spacer of variable thickness spatially separated the QW from the Ag nanostructures on top of the QW structure, which was capable of revealing subsequent energy transfer processes.

2. Fabrications and evaluations of $Cd_xZn_{1-x}O$ QWs

Single $Cd_{0.08}Zn_{0.92}O$/ZnO quantum wells (QWs) were deposited on O-polar ZnO (000-1) substrates using a pulsed laser deposition method [30]. ArF excimer laser pulses (193 nm, 3 Hz and 1 J/cm²) were focused on Cd-rich $Cd_{0.50}Zn_{0.50}O$ ceramic targets in an oxygen flow of 10^{-5} mbar. The Cd content in the well was precisely confirmed by a Rutherford backscattering technique. A $Cd_{0.08}Zn_{0.92}O$ well layer was embedded between a 100-nm thick ZnO buffer layer and a 5-nm thick ZnO capping layer. The ZnO buffer and capping layers were deposited at 650 and 270°C, respectively. The low growth temperature of the capping ZnO layer avoids any annealing effects that may occur at high temperature.

The cross-sectional images of scanning transmittance electron microscopy (STEM) revealed the local structure of a QW with a well width (L_W) of 3.2 nm (**Figure 1(a)**). According to the *Z*-contrast image of STEM, the layer with a brighter contrast indicated a $Cd_{0.08}Zn_{0.92}O$ well, whereas the darker layers presented ZnO barrier layers. The heterointerface between the well and buffer layers in the QW was found to be smooth. However, *ex situ* atomic force microscopy (AFM) observations exhibited that the ZnO buffer layer consisted of hexagonal island structures composed of regular terraces and equal width (**Figure 1(c)**), whereas the surface of the well layer possessed small island structures with a roughness height of 1.5 nm (**Figure 1(b)**). The capping/well and well/buffer heterointerfaces were not smooth at the atomic scale.

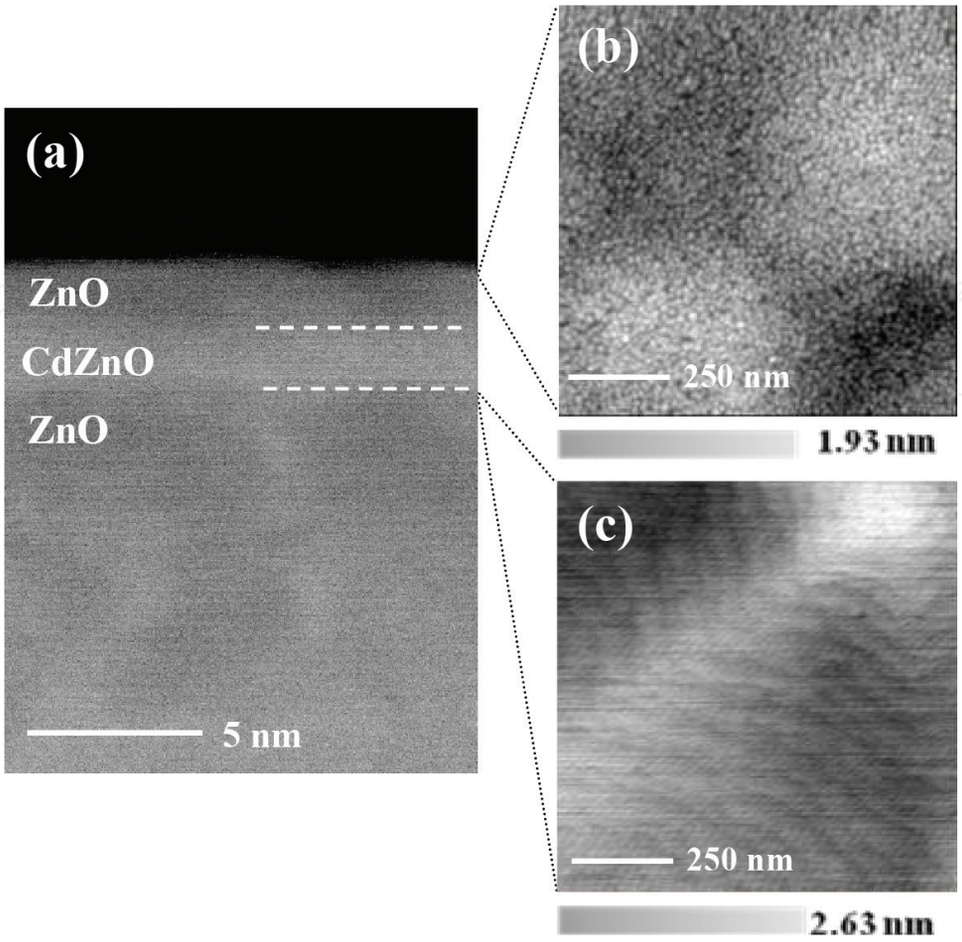

Figure 1. (a) Cross-section STEM image of the QW with a L_W of 3.2 nm. Surface AFM images of the QW with a L_W of 3.2 nm (b) and the ZnO buffer layer grown at T_g of 650°C (c). (**Figure 3** of [23]). Copyright 2011 by the American Institute of Physics.

3. Optical and structural properties of assembled Ag nanoparticles

Figure 2(a) shows a surface AFM image for the Ag structure fabricated on the QW. Ag layer consisted of small nanoparticles. The homogeneity of assembled Ag NPs was identified from a fast Fourier transform pattern (inset of **Figure 2(a)**). The extinction spectrum of the Ag NP layer showed a peak top at 2.60 eV, relating to a LSP resonance (**Figure 2(b)**) [31]. The photon energy of the LSP overlapped with that of the QW emission. This can produce an efficient energy interaction between the LSP and the QW. In addition, the reflection spectra in **Figure 2(c)** revealed that the Ag NP layer exhibited weak reflection intensity at 2.60 eV, i.e., the extinction of the Ag NP layer was almost dominated not by light scattering but by absorption. These optical properties were derived from a LSP field generated on the Ag NP layer surface [32]. Therefore, an increase of light absorption in the QW due to light extraction by reflection from the metal "mirror" is very small.

Figure 3(a) shows the cross-section TEM image of local structure of the $Cd_{0.08}Zn_{0.92}O$ QW and the Ag NP layer at atomic scale. No threading dislocation was seen at the interface between the buffer layer and the substrate. A detailed structure of the Ag NP layer was clearly obtained.

http://dx.doi.org/10.5772/intechopen.71466

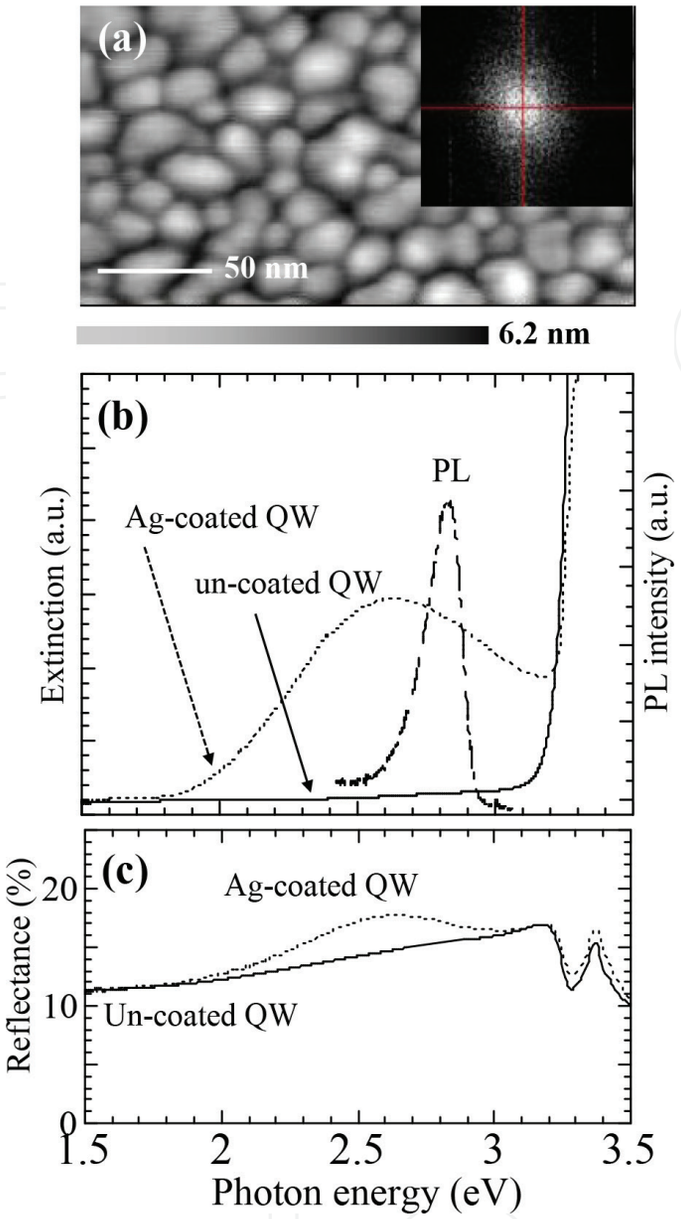

Figure 2. (a) An AFM image of an Ag-coated QW surfaces. The inset image indicates a fast Fourier transform (FFT) pattern. (b) Extinction spectra of uncoated (straight line) and Ag-coated QW (dot line) at room temperature (RT). The dot-straight line represents a PL spectrum of uncoated QW. (c) Reflectance spectra of uncoated (straight line) and Ag-coated QWs (dot line) taken at RT.

Figure 3(b) shows a cross-section TEM image focused on a heterointerface between Ag NP and ZnO layers. The Ag NP layer was composed of homogeneous alignment structure of Ag NPs with lateral and vertical sizes of 20 nm. Each Ag NP was directly located on the ZnO capping layer with a very flat surface. No thin-layered Ag nanostructure was found at the interface. In an effort to measure the local structure of the QW, a STEM was used to observe a Z-contrast image. Spatial separation between the QW and the Ag NP layer was clearly identified. The interface of the well and capping layers was found to be smooth. This also indicated that excited carriers generated in the QW were spatially separated from the Ag NP layer at nanoscale.

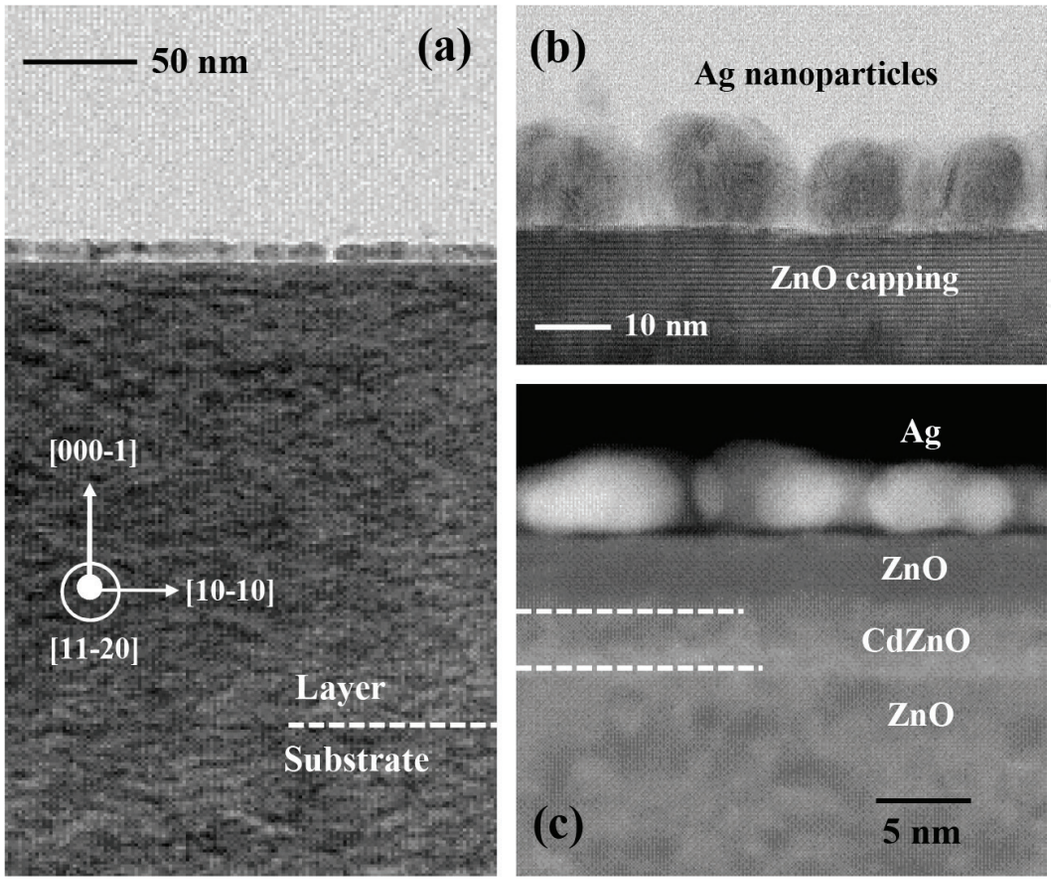

Figure 3. (a) Cross-section TEM image of the QW with Ag NP layer. (b) Cross-section TEM image at an Ag-ZnO heterointerface. (c) High-resolution STEM image focused on the QW region (**Figure 1** of [33]). Copyright [2011] the Optical Society of America.

4. PL modulation and excitonic localization

Figure 4(a) shows the steady-state PL spectra of uncoated and Ag-coated $Cd_{0.08}Zn_{0.92}O$ QW as a function of temperature. A cw InGaN laser (403 nm) was selected as excitation source to perform steady-state PL of light emission from the QW. The luminescence is dispersed by a single monochromator glazed at 500 nm. The PL intensity was dependent on the presence of Ag NP layer. At a temperature of 10 K with the Ag-coated QW, the intensity of the PL emission from the QW (hv = 2.678 eV) markedly decreased by over one order of magnitude. The quenching effect became smaller with increasing temperature and then completely vanished at 300 K (**Figure 4(b)**). **Figure 4(c)** shows the PL intensity ratio (I_{PL}^*/I_{PL}) of uncoated (I_{PL}) and Ag-coated (I_{PL}^*) QWs at different temperatures. I_{PL}^*/I_{PL} ratio increased quickly in low temperatures below 80 K and then reached as high as 92% at 10 K. This result correlated with recombination processes of excited carriers in the QW. The PL peak energy from the uncoated QW showed an *S*-shaped temperature dependence indicated localizations of excitons in the QW, which were derived from spatial Cd fluctuations and interface roughnesses (black dots in **Figure 4(c)**). If a Gaussian-like distribution of the density of state (DOS) for the conduction

http://dx.doi.org/10.5772/intechopen.71466

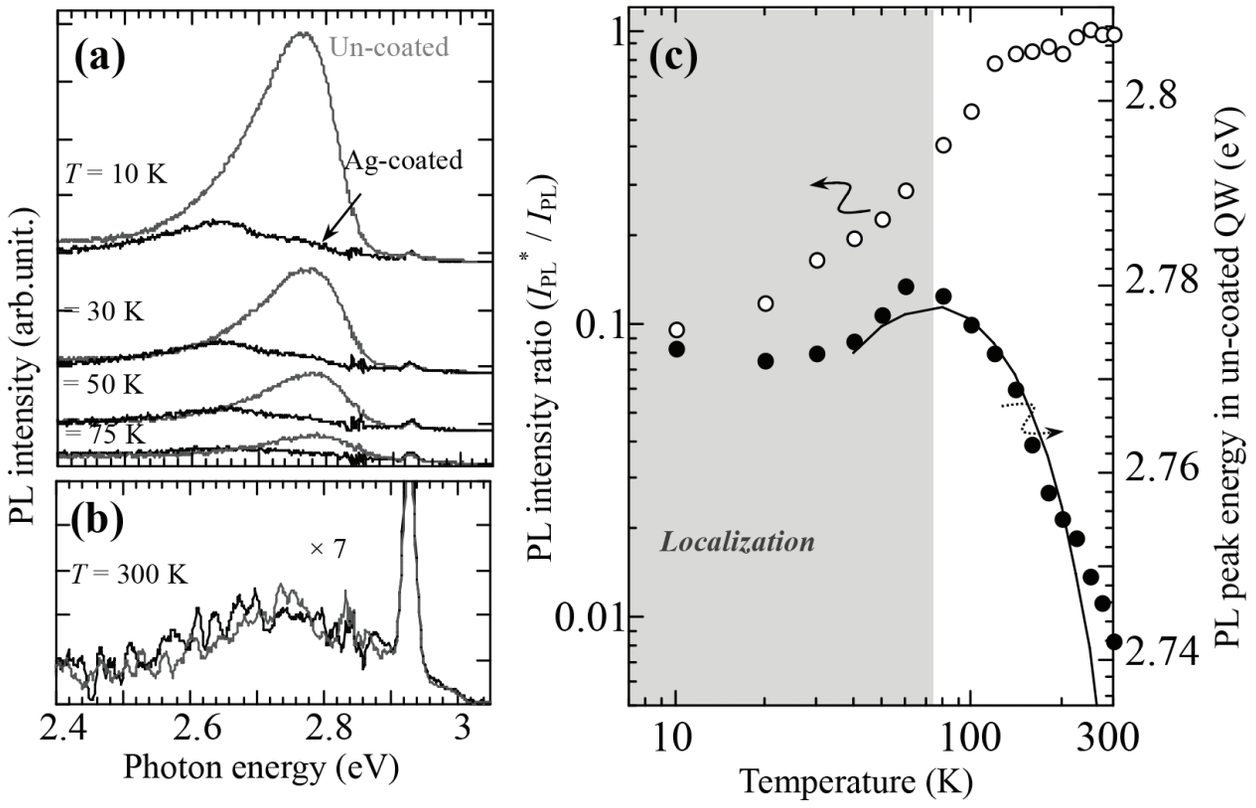

Figure 4. (a) and (b) PL spectra of uncoated (gray) and Ag-coated (black) QWs at different temperatures. (c) Open circles indicate the temperature dependence of the PL intensity ratio (I_{PL}^*/I_{PL}). Closed circles show the temperature dependence of the PL energy of the uncoated QW. The straight line indicates the Varshni equation: $E_g(T) = E_g(0) - \alpha T^2/(\beta + T)$, where T is the temperature in kelvin, $E_g(0)$ is the band gap at 0 K, and α and β are constants. Values of $E_g(0)$, α, and β were estimated as 2.793 eV, 7.6 meV, and 750 K, respectively. (**Figure 2** of [33]). Copyright [2011] the Optical Society of America.

and valence band is assumed, the *S*-shaped shift was parameter fitted by the following relation with the local amplitude of the potential fluctuations (σ) of 8 meV [34];

$$E(T) = E - \frac{\alpha T^2}{T+\beta} - \frac{\sigma^2}{k_B T} \quad (1)$$

where E represents the energy band gap at 10 K. α and β are Varshni parameters. When $k_B T$ is smaller than the local amplitude of a potential fluctuation at low temperatures, the excitons are trapped in local potential minima. Excited carriers were trapped in localized states at low temperatures below 80 K in order to form localized excitons for radiative recombination. On the other hand, excited carriers are free to escape from the localized states at high temperatures above 80 K. An electron-hole pair is not sufficiently strong to form a localized exciton. Therefore, a nonradiative recombination process dominates carrier relaxation. The starting temperature of PL quenching was close to the temperature at which excitonic localization occurred. To study optical dynamics, we monitored the temporal evolution of PL in the QW by a time-correlated single-photon counting system that provides a time resolution of 80 ps. The sample was excited at 400 nm by 2 ps pulses of the frequency-doublet output of an amplified Ti:sapphire laser. The light emission from the QW was selected by a

monochromator. The pump excitation energy was chosen to be below the band gap of ZnO, so that electrons and holes were generated only in the well. PL excitation and emission collection were carried out from the substrate side at various temperatures.

Figure 5(a) shows the time-resolved PL (TRPL) signals at 10 K taken at the PL peak energy of the uncoated and Ag-coated QWs. The TRPL signals obeyed bi-exponential decays

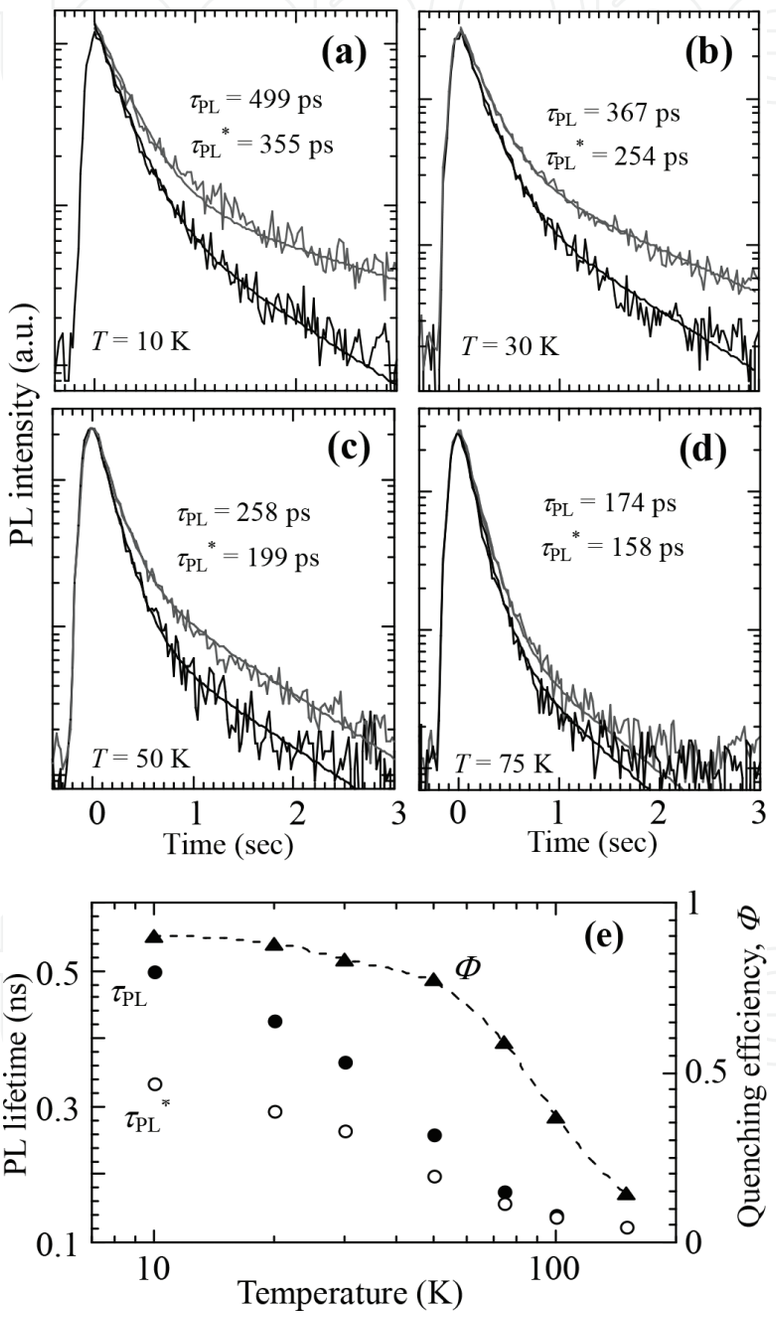

Figure 5. TRPL signals of uncoated and Ag-coated QWs at 10 K (a), 30 K (b), 50 K (c), and 75 K (d). Solid lines are fitted with bi-exponential decays represented by $I(t) = \Sigma_{i=1,2} I_i \exp.(-t/\tau_i)$, where τ_i^{-1} and I_i are the lifetime and amplitude, respectively. (e) Temperature dependence of PL lifetime for uncoated (τ_{PL}: Closed dots) and Ag-coated (τ_{PL}^*: Open dots) QWs. Closed squares indicate the quenching efficiency ($Q = 1 - I_{PL}^*/I_{PL}$).

represented by $I(t) = \Sigma_{i=1,2} I_i \exp.(-t/\tau_i)$, where τ_i^{-1} and I_i are the lifetime and amplitude, respectively. From the fitting results of the uncoated QW (gray lines), the fast decay component τ_1 (266 ps) represents a PL lifetime of the QW, whereas the slow decay component τ_2 (2.09 ns) is related to trapping and de-trapping of carriers. In contrast, the τ_1 and τ_2 values of the Ag-coated QW were similarly determined as 242 ps and 1.75 ns, respectively. The PL lifetime obtained by $(I_1\tau_1 + I_2\tau_2)/(I_1 + I_2)$ showed that τ_{PL}^* (335 ps) of the Ag-coated QW was shorter than τ_{PL} (499 ps) of the uncoated QW (black lines). The TRPL signals at 30 and 50 K were described by the bi-exponential decays (**Figure 5(b)** and **5(c)**). However, the difference in TRPL signals became small at 75 K (**Figure 5(b)**). All values of τ_{PL} and τ_{PL}^* as a function of temperature are given in **Figure 5(e)**. The difference between τ_{PL}^* and τ_{PL} became small with increasing temperature and then vanished at 100 K, which was correlated with the quenching efficiency of PL ($\Phi = 1 - I_{PL}^*/I_{PL}$) (**Figure 5(e)**). The difference between τ_{PL} and τ_{PL}^* was found for the temperature ranges in which excitonic localization occurred. However, both PL lifetimes gave the same values at the high temperatures, at which delocalization of excitons was started. The difference in the PL intensity and lifetime between uncoated and Ag-coated QWs was simultaneously observed, which indicates that energy coupling between the QW and LSP should be more effective at low temperatures.

5. Nonradiative energy transfer

For the uncoated QW, excited carriers undergo by radiative (k_R) or nonradiative (k_{NR}) decay rates. Quantum efficiency (Φ_{int}) is determined by the ratio of these two decay rates as $\eta_{int} = k_R/(k_R + k_{NR})$. In the Ag-coated QW, in contrast, new relaxation process becomes possible due to the presence of the additional electronic system of the Ag NP layer. It is for this reason that the PL decay rate of the Ag-coated QW is faster than the uncoated QW. This situation could involve a nonradiative energy transfer. The added electronic states of a metallic nanosystem offer new relaxation pathways. This relaxation should be quite effective in PL quenching as the recombination energy of excitons in the QW overlapped with the LSP absorption [35]. In this case, exciton-plasmon coupling leads to a rapid annihilation of the exciton and creation of the plasmon. Such a process gives rise to the nonradiative decay rate (k_{ET}) in carrier relaxation processes of the QW [35]. The τ_{PL}^* for the Ag-coated QW is described by the following relation:

$$\tau_{PL}^* = \frac{1}{k_{PL}^*} = \frac{1}{k_R + k_{NR} + k_{ET}} \tag{2}$$

The k_{ET} parameter is estimated from the difference in PL decay rates of the QW in the presence and absence of the Ag layer: $k_{ET} = k_{PL}^* - k_{PL}$. In **Figure 6(a)**, the temperature dependence of k_R, k_{NR}, and k_{ET} is plotted for the uncoated QW. k_R and k_{NR} rates are calculated from the relationships $k_R = k_{PL}/\Phi_{int}$ and $k_{NR} = k_{PL}(1 - \Phi_{int})$ with the quantum yield (Φ_{int}) of the uncoated QW. Φ_{int} is defined as the PL intensity at a particular temperature divided by that at 8 K (Φ_{int}: 1.3% at

300 K). At 10 K, the value of k_{PL} (2.01 ns^{-1}) was matched by that of k_R (1.90 ns^{-1}), indicating that excitons radiatively recombined at 10 K, because the value of k_R was higher than that of k_{NR}. However, the value of k_{NR} gradually became larger than that of k_R with increasing temperature, attributing to nonradiative recombination activated by delocalization of excitons. On the other hand, the values of k_{ET} were in the order of 1.0 ns^{-1} in temperature ranges from 10 to 50 K (**Figure 6(b)**). The temperature dependence of k_{ET} was similar to that of k_R, which indicated that k_{ET} was associated with k_R. At above 75 K, k_{ET} quickly decreased with an increase of k_{NR}. The carrier relaxation processes of the QW are either radiative or nonradiative, or it may experience energy transfer. At 10 K, the energy transfer rate is fast enough to compete with the radiative decay rate of the QW, so that the radiative recombination in the QW would be partially consumed by the energy transfer to the Ag nanostructures, leading to a quenched PL. The energy transfer efficiency (η_{ET}) between the QW and Ag nanostructures was calculated using the following relation:

$$\eta_{ET} = \frac{k_{ET}}{k_{ET} + k_R} \tag{3}$$

The calculated transfer efficiency achieved was as high as 34% at 10 K and then decreased quickly at high temperatures above 75 K (**Figure 6(b)**). Thus, the long PL lifetime of the QW emission at the low temperatures can make QW-LSP coupling highly probable. However, a short PL lifetime could not provide a sufficient energy transfer rate, resulting in no change in PL intensity of the QW emission.

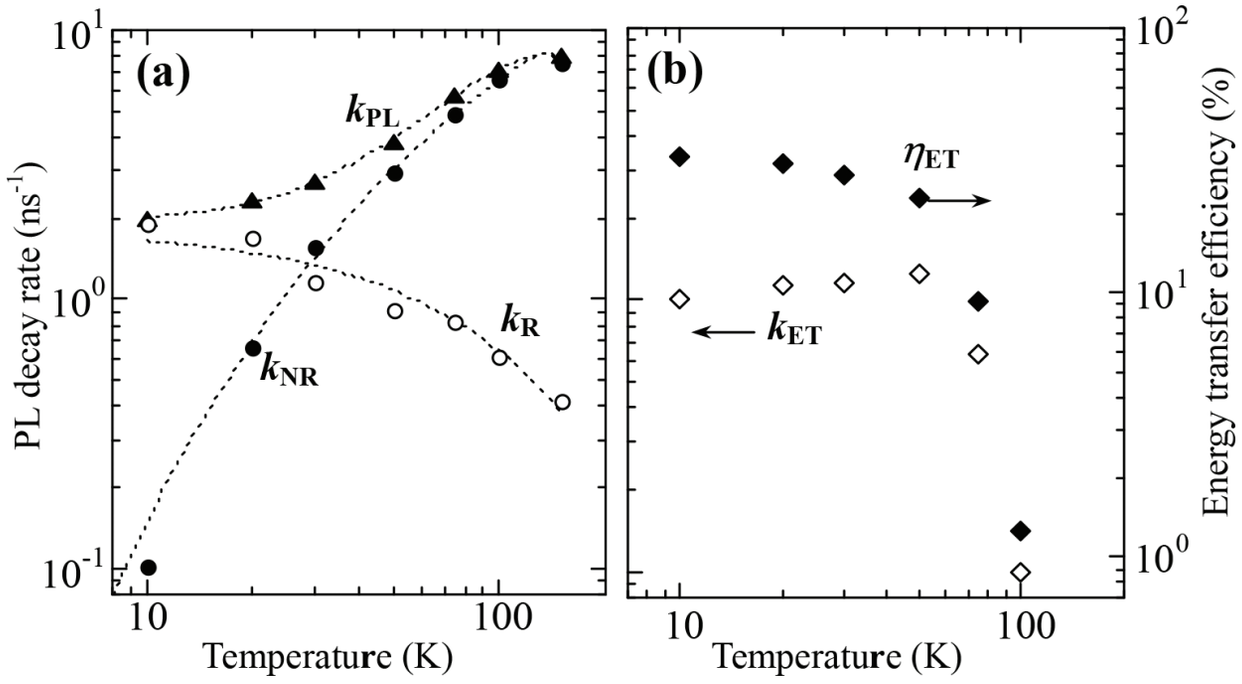

Figure 6. PL decay rate (k_{PL}: Black triangles) of the uncoated QW as a function of temperature. The open and closed circles indicate the radiative decay rate (k_R) and nonradiative decay rate (k_{NR}), respectively. Dotted lines are drawn as a visual guide. (b) Temperature dependence of the energy transfer rate (k_{ET}: Open diamonds) and efficiency of energy transfer (η_{ET}: Black diamonds). (**Figure 4** of [33]). Copyright [2011] the Optical Society of America).

http://dx.doi.org/10.5772/intechopen.71466

6. Spatial length of quenching efficiency

The relationship between a separation length (d) of the QW from the Ag NP layer and the quenching efficiency was also studied. For the Ag-coated QW, the plot of the quenching efficiency (Q) at 10 K as a function of d is shown in **Figure 7**. This length is controlled by the layer thickness of the ZnO capping layer. The narrow length of 5 nm yielded a high Q value of 92%. The dependence of Q on length was observable up to a distance of 400 Å. The energy transfer from the QW to the proximal Ag NP layer caused efficient PL quenching of the QW even at large lengths. We now consider the use of FRET and SET mechanisms applied to transfer processes of the hybrid structure of metal NPs and semiconductor QDs [13]. A FRET process that occurs between two proximity molecules (donor and acceptor) is commonly employed to explain the quenching process in regard to the quencher as the acceptor. Like dipole-dipole interactions in a FRET process, a dipole-surface energy transfer (SET) is known as metal-induced quenching. The quenching efficiency of FRET and SET processes is dependent on the spectral overlap of acceptor's absorption with the donor's emission and also affects the separation distance of between the donor and acceptor molecules. Quenching efficiency $Q(d)$ can be described by the following equations [13]:

$$Q(d) = 1 - \frac{1}{1 + \left(\frac{d}{d_0}\right)^n} \tag{4}$$

where $n = 4$ and $n = 6$ represent SET and FRET mechanisms, respectively; d_0 is the length at which the QW displays equal probabilities for energy transfer and PL emission, representing a 50% PL intensity. The experimental data (black circles) were well fitted to Eq. (1) with $n = 4$ and $d_0 = 133$ Å (straight line in **Figure 7(a)**), which was close to the theoretical value for d_0 of 103 Å, as follows [13]:

$$d_0 = \left(0.225 \frac{cn^2}{(2\pi)^2 \omega_f k_f} \Phi_{em} \lambda_{QW}^2\right)^{1/4} \tag{5}$$

where c is the speed of light in a vacuum, n is the index of refraction of the medium (1.95 in ZnO), Φ_{em} is the quantum yield of the uncoated QW (0.96 at 10 K), λ_{QW} is the QW emission wavelength (4.47×10^{-5} cm), and ω_f and k_f are the angular frequency (8.40×10^{15} cm^{-1}) and Fermi wave vector (1.20×10^{8} cm^{-1}) for Ag, respectively. The PL quenching due to energy transfer from the QW to Ag NP layer obeyed a SET process with d^{-4} dependence.

Previous studies on quenching related to metallic-induced luminescence have suggested two different models. One is the contact model proposed by Choosing *et al.* [36], in which the luminescent quench was associated with the diffusion of excitons in the organic film to the metal/organic interface. The other is the noncontact model of Chance *et al.* [37] based on interactions between organic dipoles (excited organic molecules) and electron gas (electron-hole pairs) in metal, which would induce energy transfer from the organic to the metal surface. Electron-hole pairs in metal are generated through relaxation processes

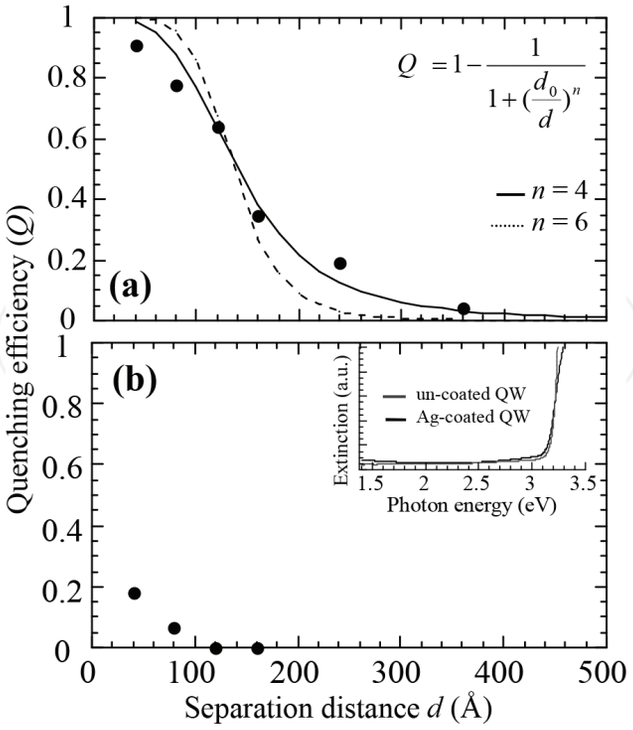

Figure 7. (a) Quenching efficiency (Q) at 10 K as a function of the separation length (d) between the QW and Ag NP layer (black dots). The straight and dot lines are theoretically fitted with n = 4 and 6 using Eq. (4), respectively. (b) the values of Q at 10 K a function of d between the QW and flat Ag layer fabricated by a RF sputtering technique (black triangles). The inset figures indicate extinction spectra taken at RT of uncoated (gray) and Ag-coated QWs (black) fabricated using the flat Ag layer.

of plasmon resonances, which operate as quenchers of luminescence. In our case, excitonic emissions from the QWs could be considered as dipole emitters, which were energetically suppressed by electron-hole pairs related to the LSPs on the Ag NP layers. That is, the Ag-coated QWs did not obey a FRET process with a dipole-dipole interaction but a SET process with a dipole-surface interaction. This represents the fact that the oscillating dipoles in the QW are coupled directly with the free carriers (electron and holes) on the layer surface of Ag NPs. From AFM and TEM images, the Ag NP layer showed a large surface area, producing high surface energy. It was thought that the LSP resonance induced on the surface of the Ag NP layer enhanced the quenching efficiency of PL. Slight difference between experimental (closed dots) and theoretical data (straight line) is related to structural imperfections. As shown in **Figure 3**, inhomogeneity of spatial distance between the QW and Ag NP layer was observed, which affects quenching efficiency as a function of separation distance.

As another aspect, participation of the LSP involving the PL quenching was explored using a flat Ag layer. The RD-sputtered Ag layer showed a very flat surface with a roughness of 1 nm and had no LSP absorption (inset of **Figure 7(b)**). In this case, the value of Q was as small as 18% at a short length of 5 nm and then quickly decreased down to zero at a distance of 12 nm (**Figure 7(b)**). The comparative study revealed that the LSP absorption played a determinant role in increasing quenching efficiency of PL.

7. Discussion

The PL enhancement of $In_xGa_{1-x}N$/GaN QWs with Ag nanostructures has been observed near room temperature (RT), relating to the electronic states in the QWs. Lu *et al*. reported that transfer probability to a SP mode of a pair of trapped carriers "localized excitons" is significantly lower than that of a pair of free carriers [25]. They insisted that localization of carriers with decreasing temperature suppressed the QW-SP coupling rate. In addition, Okamoto *et al.* showed that the temperature dependence of the QW-SP coupling rate was similar to that of nonradiative decay rate [24]. Their prior reports imply that the QW-SP coupling is enhanced, when the QW has electronic states consisting of free electrons and holes, which gives effective energy transfer for PL enhancement. Energy of free carriers excited in the QW is directly coupled to an SP mode. This concept can be also applicable to an energy transfer process from a semiconductor QW to a proximal monolayer of a semiconductor QD (or an organic dye) based on $In_xGa_{1-x}N$ QWs [38, 39]. This transfer efficiency enhances with increasing temperature, relating to a change of electronic states in a QW from trapped carriers to free carriers. The above precedent indicates that the energy of free carriers excited in a QW is indispensable for being resonant with an SP mode or a QD.

In contrast, PL quenching of the $Cd_xZn_{1-x}O$ QW with Ag NP layer in this work showed the opposite tendency. The transfer efficiency enhanced with decreasing temperature. The temperature dependence of the energy transfer rate was similar to that of the radiative decay rate (**Figure 6(a)** and **6(b)**). Therefore, the recombination energy of localized excitons in the QW is partially consumed by nonradiative energy transfer to the Ag NP layer, resulting in quenching PL. This originates from an overlap of photon energy between the QW emission and the LSP absorption. This situation has been also observed on Au NP–CdSe QDs [40]. The difference in energy transfer processes between PL enhancement and quenching is attributed to electronic states in a QW placed in vicinity of metallic nanostructures, that is, localization or delocalization of excited carriers. It is suggested that radiative QW emission due to excitonic localization contributes to PL quenching, which supported the past reports that PL suppression became strong with decreasing temperature as well as with increasing quantum efficiency on $In_xGa_{1-x}N$ QWs. The prevention of localized excitons in the QW would be desired to reduce PL quenching phenomenon if possible toward efficient plasmon-coupled emitting devices.

8. Conclusion

The remarkable PL quenching in the hybrid structure of $Cd_xZn_{1-x}O$ QW with Ag NP layer was observed at low temperatures, which was strongly dependent on the electronic states in the QW. The quenching effect was found in the temperature region in which excited carriers radiatively recombined owing to excitonic localization. On the other hand, delocalization of excitons with increasing temperature led to a decreased quenching efficiency. Energy transfer for the PL quenching was generated when the photon energy of the QW emission overlapped with that of LSP absorption. In addition, the spatial separation of the QW from the Ag NP layer revealed that the PL quenching showed a long-range length obeyed almost, which could be explained by a SET process. The comparative study used the Ag NP layers with different character clarified that the

origin of PL quenching was attributed to the local LSP field induced on Ag NP layer. As a consequence, it was indicated that QW-LSP coupling played an important role in quenching PL. This coupling required existence of a pair of trapped carriers "localized excitons" as an electronic state in the QW. On the other hand, the quenching effect was not observed at the high temperatures at which excited carriers exist as free electrons and holes in the QW. Then, QW emission was dominated by a decay rate that was exhibited in the PL as a nonradiative contribution. It was identified that the electronic states of a QW played an important role in quenching PL.

Acknowledgements

This research was supported by a grant-in-Aid for Exploratory Research (No. 15 K13331) and Scientific Research (B) (No. 25289084).

Author details

Hiroaki Matsui[1,2]*

*Address all correspondence to: hiroaki@ee.t.u-tokyo.ac.jp

1 Department of Bioengineering, University of Tokyo, Tokyo, Japan

2 Department of Electric Engineering and Information Systems, University of Tokyo, Tokyo, Japan

References

[1] Wing WJ, Sadeghi SM, Gutha RR, Campbell Q, Mao C. Metallic nanoparticle shape and size effects on aluminum oxide-induced enhancement of exciton-plasmon coupling and quantum dot emission. Journal of Applied Physics. 2015;**118**:124302(1-5). DOI: 10.1063/1.4931378

[2] Gao H, Teng J, Chua SJ. Simultaneous coupling of surface plasmon resonance and photonic band gap to InGaAs quantum well emission. Journal of Applied Physics. 2016;**119**:013104(1-6). DOI: 10.1063/1.4939502

[3] Li Y, Liu B, Zhang R, Xie Z, Zhuang Z. Investigation of surface-plasmon coupled red light emitting InGaN/GaN multi-quantum well with Ag nanostructures coated on GaN surface. Journal of Applied Physics. 2015;**117**:153103(1-5). DOI: 10.1063/1.4918555

[4] Bellessa J, Symonds C, Meynaud C, Plenet JC, Cambril E, Miard A, Ferlazzo L. Exciton/plasmon polaritons in GaAs/Al0.93Ga0.07As heterostructures near a metallic layer. Physical Review B. 2008;**78**:205326(1-4). DOI: 10.1103/PhysRevB78.205326

[5] Okamoto K, Niki I, Shvartser A, Narukawa Y, Mukai T. Surface-plasmon-enhanced light emitters based on InGaN quantum wells. Nature Materials. 2004;**3**:601-605. DOI: 10.1038/namt1198

[6] Neogi A, Morkoç H, Kuroda T, Takeuchi A. Coupling of spontaneous emission from GaN-AlN quantum dots into silver surface Plasmons. Optics Letters. 2005;**30**:93-95. DOI: 10.1364/OL.30.000093

[7] Chance RP, Prock A, Sibey R. Molecular florescence and energy transfer near interfaces. Advances in Chemical Physics. 2007;**37**:1-65. DOI: 10.1002/9780470142561.ch1

[8] Gebauer W, Langner A, Schneider M, Sokolowski M, Umbach E. Luminescence quenching of ordered π-conjugated molecules near a metal surface: Quaterthiophene and PTCDA on Ag (111). Physical Review B. 2004;**69**:155432(1-8). DOI: 10.1103/PhysRevB.69.155431

[9] Li X, Qian J, Jang L, He S. Florescence quenching of quantum dots by gold Nanorods and its application to DNA detection. Applied Physics Letters. 2009;**94**:063111(1)-(3). DOI: 10.1063/1.3080662

[10] Hoshen EC, Bryant GW, Pinkas I, Sperling J, Bar-Joseph I. Exciton-plasmon interactions in quantum dot-gold nanoparticle structures. Nano Letters. 2012;**12**:4260-4264. DOI: 10.1021/nl301917d

[11] Akselrod GM, Weidman MC, Li Y, Argyropoulos C, Tisdale WA, Mikkelsen MH. Efficient nanosecond photoluminescence from infrared PbS quantum dots coupled to plasmonic nanoantennas. ACS Photonics. 2016;**3**:1741-1746. DOI: 10.1021/acsphotonics.6b00357

[12] Matsumoto Y, Tamitake R, Nakanishi S, Ishikawa M, Biju V. Photoluminescence quenching and intensity fluctuations of CdSe-ZnS quantum dots on an Ag nanoparticle film. Journal of Physical Chemistry C. 2008;**112**:1345-1350. DOI: 10.1021/jp076659+

[13] Pons T, Medintz IL, Sapsford KE, Higashiya S, Grimes AF, English DS, Mattoussi H. On the quenching of semiconductor quantum dot photoluminescence by proximal gold nanoparticles. Nano Letters. 2007;**7**:3157-3164. DOI: 10.1021/nl071729+

[14] Viste P, Plain J, Jaffiol R, Vial A, Adam PM, Royer P. Enhancement and quenching regimes in metal-semiconductor hybrid optical nanosources. ACS Nano. 2010;**4**:759-764. DOI: 10.1021/nn901294d

[15] Gueroui Z, Libchaber A. Single-molecule measurements of gold-quenched quantum dots. Physical Review Letters. 2004;**93**:166108(1-4). DOI: 10.1103/PhysRevLett93.166108

[16] Förster T. 10th Spiers memorial lecture. Transfer mechanisms of electronic excitation. Discuss Faraday Society. 1959;**27**:7-17. DOI: 10.1039/DF9592700007

[17] Jennings TL, Singh MP, Strouse GF. Fluorescent lifetime quenching near d = 1.5 nm gold nanoparticles: Probing NSET validity. Journal of the American Society. 2006;**128**:5462-5467. DOI: 10.1021/ja0583665

[18] Henson J, Heckel JC, Dimakis E, Abell J, Bhattacharyya A. Plasmon enhanced light emission from InGaN quantum wells via coupling to chemically synthesized silver nanoparticles. Applied Physics Letters. 2009;**95**:151109(1-3). DOI: 10.1063/1.3249579

[19] Liu B, Cheng CW, Chen R, Ekahana A, Yang WF. Surface plasmon induced exciton redistribution in ZnCdO/ZnO coaxial multi-quantum-well nanowires. Applied Physics Letters. 2010;**97**:081107(1-3). DOI: 10.1063/1.3480414

[20] Chen CY, Yeh DM, Lu YC, Yang CC. Dependence of resonant coupling between surface plasmons and InGaN quantum wells on metallic structure. Applied Physics Letters. 2006;**89**:203113(1-3). DOI: 10.1063/1.2390639

[21] Estrin Y, Rich DH, Keller S, DenBaars SP. Temperature dependence of exciton-surface plasmon polariton coupling in Ag, au and au films on $In_xInGa_{1-x}N$/GaN quantum wells studied with time-resolved cathodoluminescence. Journal of Applied Physics. 2015;**117**:043105(1-14). DOI: 10.1063/1.4906850

[22] Chichibu SF, Onuma T, Aoyama T, Nakajima K, Ahmet P, Chikyow T, Sota T, DenBaars SP, Nakamura S, Kitamura T, Ishida Y, Okuyama H. Recombination dynamics of localized excitons in cubic $In_xGa_{1-x}N$/GaN multiple quantum wells grown by radio frequency molecular beam epitaxy on 3C-SiC substrate. Journal of Vacuum Science and Technology B. 2003;**21**:1856-1862. DOI: 10.1116/1.1593645

[23] Matsui H, Osone T, Tabata H. Band alignment and excitonic localization of ZnO/Cd0.08Zn0.92O quantum wells. Journal of Applied Physics. 2010;**107**:093523(1-7). DOI: 10.1063/1.3359720

[24] Okamoto K, Niki I, Scherer A, Narukawa Y, Mukai T, Kawakami Y. Surface plasmon enhanced spontaneous emission rate of InGaN/GaN quantum wells probed by time-resolved photoluminescence spectroscopy. Applied Physics Letters. 2005;**87**:071102(1-3). DOI: 10.1063/1.2010602

[25] Lu YC, Chen CY, Yeh DM, Huang CF, Tang TY. Temperature dependence of surface plasmon coupling with an InGaN/GaN quantum well. Applied Physics Letters. 2007;**90**:193103(1-3). DOI: 10.1063/1.2738194

[26] Matsui H, Tabata H. The contribution of quantum confinement to optical anisotropy of A-plane $Cd_{0.06}Zn_{0.94}O$/ZnO quantum wells. Applied Physics Letters. 2012;**100**:171910(1-3) 10.1063/1.4707384

[27] Matsui H, Tabata H. In-plane light polarization in nonpolar M-plane $Cd_xZn_{1-x}O$/ZnO quantum wells. Applied Physics Letters. 2011;**98**:261902(1-3). DOI: 10.1063/1.3603931

[28] Matsui H, Tabata H. In-plane anisotropy of polarized photoluminescence in M-plane (10-10) ZnO and MgZnO/ZnO multiple quantum wells. Applied Physics Letters. 2009;**94**: 161907(1-3). DOI: 10.1063/1.3124243

[29] Matsui H, Tabata H. Critical thickness and lattice relaxation of mg-rich strained $Mg_{0.37}Zn_{0.63}O$ (0001) layers towards multi-quantum wells. Journal of Applied Physics. 2006;**99**:024902(1)-(6). DOI: 10.1063/1.2161422

[30] Matsui H, Saeki H, Kawai T, Sasaki A, Yoshimoto M, Tsubaki M, Tabata H. Characteristics of polarity-controlled ZnO films fabricated using the homoepitaxy technique. Journal of Vacuum Science and Technology. 2004;**22**:2454-2460. DOI: 10.1116/1.792237

[31] Donnelly T, Doggett B, Lunney JG. Pulsed laser deposition of nanostructured Ag films. Applied Surface Science. 2006;**252**:4445-4448. DOI: 10.1016/apsusc.2005.048

[32] Matsuda K, Ito Y, Kanemitsu Y. Photoluminescence enhancement and quenching of single CdSe/ZnS nanocrystals on metal surfaces dominated by Plasmon resonant energy transfer. Applied Physics Letters. 2008;**92**:211911(1-3). DOI: 10.1063/1.2937142

[33] Matsui H, Nomura W, Yatsui T, Ohtsu M, Tabata H. Optical dynamics of energy-transfer from a CdZnO quantum well to a proximal Ag nanostructure. Optics Letters. 2011;**36**:3735-3737. DOI: 10.1364/OL.36.003735

[34] Bai J, Wang T, Sakai S. Influence of the quantum –well thickness on the radiative recombination of InGaN/GaN quantum well structures. Journal of Applied Physics. 2000;**88**:4729-4734. DOI: 10.1063/1.311831

[35] Neretina S, Qian W, Dreaden E, El-Sayed MA, Hughes RA, Preston JS, Mascher P. Nano Letters. Plasmon Field Effects on the Nonradiative Relaxation of Hot Electrons in an Electronically Quantized System: CdTe-Au Core-Shell Nanowires. 2008;**8**:2410

[36] Choong V, Park Y, Gao Y, Wehrmmeister T, Müllen K, Hsieh BR, Tang CW. Dramatic photoluminescence quenching of phenylene vinylene oligomer thin films upon submonolayer Ca deposition. Applied Physics Letters. 1996;**71**:1492-1494. DOI: 10.1063/1.116918

[37] Neretina S, Qian W, Dreden E, El-Sayed MA, Hughes RA, Preston JS, Mascher P. Plasmon field effects on the nonradiative relaxation of hot electrons in an electronically quantized system: CdTe-au core-shell nanowires. Nano Letters. 2008;**8**:2410-2418. DOI: 10.1021/nl801303g

[38] Kos Š, Achermann M, Klimov VI, Smith DL. Different regimes of Förster-type energy transfer between an epitaxial quantum well and a proximal monolayer of semiconductor nanocrystals. Physical Review B. 2005;**71**:205309(1-8). DOI: 10.1103/PhysRevB71.205309

[39] Blumstengel S, Sadofev S, Xu C, Puls J, Henneberger F. Converting Wannier into Frenkel excitons in an inorganic/organic hybrid semiconductor nanostructure. Physical Review Letters. 2006;**97**:237401(1-4). DOI: 10.1103/PhysRevLett97.237401

[40] Haridas M, Tripathi LN, Basua JK. Photoluminescence enhancement and quenching in metal-semiconductor quantum dot hybrid arrays. Applied Physics Letters. 2011;**98**:063305(1-3). DOI: 10.1063/1.3553766

IntechOpen